

Propagating and evanescent properties of double-point defects in Sonic Crystals

V. Romero-García^{1,2}, J.V. Sánchez-Pérez¹ and L.M. Garcia-Raffi³.

¹ Centro de tecnologías físicas: Acústica, Materiales y Astrofísica, Universidad Politécnica de Valencia, Camino de Vera s/n, 46022 Valencia

² Instituto de Ciencia de los Materiales. Consejo Superior de Investigaciones Científicas. Sor Juana Ins de la Cruz, 3, Cantoblanco, 28049, Madrid, Spain.

³ Instituto Universitario de Matemática Pura y Aplicada, Universidad Politécnica de Valencia, Camino de Vera s/n, 46022 Valencia

E-mail: virogar1@mat.upv.es

Abstract. Complex Band Structures and Multiple Scattering Theory have been used in this paper to analyze the overlapping of the evanescent waves localized in point defects in Sonic Crystals. The Extended Plane Wave Expansion (EPWE) with supercell approximation gives the imaginary part of the Bloch vectors that produces the decay of the localized modes inside the periodic system. Double-cavities can present a coupling between the evanescent modes localized in the defect, showing a symmetric or antisymmetric modes. When point defects are close, the complex band structures reveal a splitting of the frequencies of the localized modes. Both the real part and the imaginary values of k of the localized modes in the cavities present different values for each localized mode, which gives different properties for each mode. Novel measurements, in very good agreement with analytical data, show the experimental evidences of the symmetric and antisymmetric localized modes for a double-point defect in Sonic Crystals (SC). The investigation on the localization phenomena and the coupling between defects in periodic systems has a fundamental importance both in pure and in applied physics.

PACS numbers: 43.20.+g, 43.35.+d, 63.20.D-, 63.20.Pw

1. Introduction

Periodic distributions of elastic scatterers in an elastic host medium with different physical properties are known as Phononic Crystals (PC) [1, 2] and they are the elastic analogous of the well-known Photonic Crystals [3, 4]. If one of the materials in PC is a fluid, then the system is called Sonic Crystal (SC) [5]. All of these systems present interesting physical properties and recently they have received increasing attention mainly due to the great number of applications in several branches of physics and engineering [6, 7, 8]. One of the most important properties of these inhomogeneous materials are the so-called Band Gaps (BG): frequency ranges where waves do not propagate through the periodic system. The existence of these BG leads to a several applications, for instance, in the case of SC as acoustic filters [9, 10], acoustic barriers [11] or waveguides [12], among others.

In periodic systems Bloch's theorem and Fourier expansion of the periodic physical properties, transform the acoustic wave equation in an eigenvalue problem. The eigenfrequencies $\omega(k)$ for each Bloch's vector k inside the irreducible part of the first Brillouin Zone constitute the band structure. This methodology is usually called Plane Wave Expansion (PWE) [13] and it can be used to obtain the so-called band structures, i.e. the propagating modes through the periodic system. The band structures reveal that BG are ranges of frequencies where no real k exists. It has been shown that the eigenvalues of the problem have real value for the case of SC [14].

One of the most important properties of the periodic structures is the emergence of the localized modes within the BG when a point defect is introduced [9, 15]. A widely technique used in the literature to obtain the effect of the creation of point defects in crystals is the supercell approximation in PWE [10, 16, 17]. This approximation gives information only about the propagation nature of the localized modes in the point defects. In these cases when periodicity is broken or when SC have finite size, evanescent modes inside the periodic system may appear. Localized modes or modes inside the BG are characterized by its evanescent behaviour [7, 18, 19]. Then a more accurate analysis is needed to characterize all the properties of the modes inside the periodic system.

A wave impinging on a complete periodic system with a given frequency ω inside the BG, is characterized by complex valued wave numbers $k(\omega)$ which represent the multiexponential decay of the evanescent mode inside the periodic system [18]. Recent works [20, 21, 22] show an extension of the Plane Wave Expansion (Extended Plane Wave Expansion (EPWE)) obtaining the complex part of the Bloch's waves revealing that the decay of the modes inside the BG grows as the frequency reaches the center of the BG. In this sense a localization factor has been defined recently to show this behaviour [23]. The localization factor can be also related with recent results that show that, although the decay of these localized modes is multi-exponential, it can be approximated by an exponential like decay considering only the first harmonic of the Bloch waves in SC made of rigid cylinders [19].

On the other hand, Sainidou et al. [24] have introduced a novel extension of the

Multiple Scattering Theory [25] for analyzing slabs which consist of slices of different material as long as the periodicity parallel to the surface of the slab is preserved. The method, called Layer Multiple Scattering (LMS) allows to study the scattering problem of slabs that are finite in the direction parallel to the surface of the slab, but infinite in the normal directions to this surface. Alternatively, one can use this method to calculate the complex phononic band structures of an infinite crystal, associated with a given crystallographic plane. In this case the method provides the propagating and evanescent Bloch waves of the elastic field in the given crystal, corresponding to a given k and a given frequency. LMS has been used to analyze the guidance and quasiguide of elastic waves in a glass plate coated on one side with a periodic monolayer of polymer spheres, immersed in water, observing the dispersion diagrams of the interacting modes of the composite slab [26].

The goal of the paper is to analyze the three main characteristics of defect modes in SC: splitting, symmetry vibrational patterns and evanescent decay of the modes. In addition to the PWE, to do this study we have used the EPWE with supercell approximation because it is fundamental for the complete understanding of the localized modes. We present the explicit matrix formulation of the supercell approximation in the EPWE for N_p point defects. From the complex and real band structures we observe the splitting, and the evanescent behaviour of the localized modes inside the BG around the defect. We analyze the localized modes inside multi-point defects, specially in the double point defect case.

MST in finite SC is used to analyze the vibrational patterns of the localized modes in a double point defect. In this case, when the distance between both defects is low enough, it appears a symmetric and antisymmetric vibrational modes similar to the case of a system formed by two masses and three springs, or to the Zeeman effect in the atomic spectra [15]. Novel experimental data that are in good agreement with theory show for first time the symmetry of the vibrational patterns of the localized modes in such a double point defect. Moreover we observe the decay of the localized modes outside the double-point defect in good agreement with the results obtained by EPWE with supercell approximation.

The paper is organized as follows. First of all we show the main ingredients of the Extended Plane Wave Expansion as well as the explicit matrix formulation of the problem and the extension for a supercell with N_p point defects. After that, it is shown the numerical, analytical and experimental results of a double-point defect, showing the complete explanation of the splitting, the symmetry of the vibrational patterns and the decay of the localized modes. Finally we show a summary as well as the main conclusions of the work.

2. Extended PWE with supercell approximation

The analysis of the propagating modes can be done by the $\omega(\vec{k})$ formulation, where the existence of BG is indicated by the absence of bands in determined ranges of frequencies.

The mechanism of creation of BG in finite crystals could be understood by the evanescent behaviour of the modes inside it. At a given frequency ω inside the BG, the evanescent wave is characterized by a complex valued Bloch vectors $\vec{k}(\omega)$ that characterize the decay of the mode inside the periodic structure. Based on the work of Hsue et al. [20] a recent work by Laude et al. [21] shows the calculation of complex band structure for phononic crystals. Recently, this work has been extended for the case of SC for calculations using the supercell approximation [22], which is specially indicated for SC with point defects. In this section we present the explicit matrix formulation of the Extended Plane Wave Expansion with supercell approximation to calculate the properties of SC with N_p point defects inside a supercell. We must take into account that PWE needs a low interaction between supercells.

$\omega(k)$ methods are characterized by the next eigenvalue problem:

$$\sum_{\vec{G}'} ((\vec{k} + \vec{G})\sigma_k(\vec{G} - \vec{G}')(\vec{k} + \vec{G}') - \omega^2\eta(\vec{G} - \vec{G}'))p_{\vec{k}}(\vec{G}') = 0. \quad (1)$$

Where \vec{G} is the 2D reciprocal-lattice vector, k is the Bloch vector and p_k is the pressure. Equation (1) constitutes a set of linear, homogeneous equations for the eigenvectors $p_{\vec{k}}(\vec{G})$ and the eigenfrequencies $\omega(\vec{k})$. We obtain the band structures letting \vec{k} scan the irreducible part of the first Brillouin zone.

Equation (1) can be expressed by the next matrix formulation [13]

$$\sum_{i=1}^3 \Gamma_i \Sigma \Gamma_i P = \omega^2 \Omega P, \quad (2)$$

where $i=1,2,3$, and

$$\Sigma = \begin{pmatrix} \sigma(\vec{G}_1 - \vec{G}_1) & \dots & \sigma(\vec{G}_1 - \vec{G}_{N \times N}) \\ \vdots & \ddots & \vdots \\ \sigma(\vec{G}_{N \times N} - \vec{G}_1) & \dots & \sigma(\vec{G}_{N \times N} - \vec{G}_{N \times N}) \end{pmatrix}, \quad (3)$$

$$\Omega = \begin{pmatrix} \eta(\vec{G}_1 - \vec{G}_1) & \dots & \eta(\vec{G}_1 - \vec{G}_{N \times N}) \\ \vdots & \ddots & \vdots \\ \eta(\vec{G}_{N \times N} - \vec{G}_1) & \dots & \eta(\vec{G}_{N \times N} - \vec{G}_{N \times N}) \end{pmatrix}, \quad (4)$$

$$P = \begin{pmatrix} P(\vec{G}_1) \\ \vdots \\ P(\vec{G}_{N \times N}) \end{pmatrix}, \quad (5)$$

where $\vec{G} = (G_1, G_2, G_3) = (2\pi m/a_1, 2\pi n/a_2, 0)$ for the case of the 2D square arrays. If we chose $m = n = (-M, \dots, M)$, the size of the previous matrices is $N \times N = (2M + 1) \times (2M + 1)$.

From equation (2) we define the next vector,

$$\Phi_i = \Sigma \Gamma_i P. \quad (6)$$

With this definition we can reformulate the eigenvalue problem (2) as the equations system

$$\begin{aligned}\Phi_i &= \Sigma \Gamma_i P \\ \omega^2 \Omega P &= \sum_{i=1}^3 \Gamma_i \Phi_i.\end{aligned}\tag{7}$$

In order to obtain an eigenvalue problem for $\vec{k}(\omega)$, we write $\vec{k} = k\vec{\alpha}$, where $\vec{\alpha}$ is a unit vector. Then Γ_i matrix can be written as

$$\Gamma_i = \Gamma_i^0 + k\alpha_i I,\tag{8}$$

where I is the identity matrix, and

$$\Gamma_i^0 = \begin{pmatrix} G_i & 0 & \dots & 0 \\ 0 & G_i & \dots & 0 \\ \vdots & \vdots & \ddots & \vdots \\ 0 & \dots & \dots & G_i \end{pmatrix},\tag{9}$$

$$\alpha_i = \begin{pmatrix} \alpha_i & 0 & \dots & 0 \\ 0 & \alpha_i & \dots & 0 \\ \vdots & \vdots & \ddots & \vdots \\ 0 & \dots & \dots & \alpha_i \end{pmatrix}.\tag{10}$$

Then, equation (2) can be written in the form of (11), where $\Phi' = \sum_{i=1}^3 \alpha_i \Phi_i$.

$$\begin{pmatrix} \omega^2 \Omega - \sum_{i=1}^3 \Gamma_i^0 \Sigma \Gamma_i^0 & 0 \\ -\sum_{i=1}^3 \Sigma \Gamma_i^0 & I \end{pmatrix} \begin{pmatrix} P \\ \Phi' \end{pmatrix} = k \begin{pmatrix} \sum_{i=1}^3 \Gamma_i^0 \Sigma \alpha_i & I \\ \sum_{i=1}^3 \Sigma \alpha_i & 0 \end{pmatrix} \begin{pmatrix} P \\ \Phi' \end{pmatrix}\tag{11}$$

Equation (11) represents a generalized eigenvalue problem with $2N$ eigenvalues k , with possibly complex values. Complex band structures on the incidence direction $\vec{\alpha}$ have been obtained by solving the eigenvalue equation for a discrete number of frequencies and then sorted by continuity of k . In contrast to the $\omega(\vec{k})$ method, in this formulation the periodicity is not relevant and $k(\omega)$ does not follow the first Brillouin zone.

We consider a SC with primitive lattice vectors \vec{a}_i ($i = 1, 2, 3$). The supercell is a cluster of $n_1 a \times n_2 a \times n_3 a$ scatterers periodically placed in the space. Then, the primitive lattice vectors in the supercell approximation are $\vec{a}'_i = n_i \vec{a}_i$, and the complete set of lattices in the supercell approximation is $\{R' | R' = l_i \vec{a}'_i\}$, where n_i and l_i are integers. The primitive reciprocal vectors are then

$$\vec{b}'_i = 2\pi \frac{\varepsilon_{ijk} \vec{a}'_j \times \vec{a}'_k}{\vec{a}'_1 \cdot (\vec{a}'_2 \times \vec{a}'_3)}\tag{12}$$

where ε_{ijk} is the three-dimensional Levi-Civita completely anti-symmetric symbol. The complete set of reciprocal lattice vectors in the supercell is $\{\vec{G} | \vec{G}_i = N_i \vec{b}'_i\}$ where N_i are integers.

The density ρ_i and the bulk modulus B_i , are the physical properties involved in the wave equation and using the Fourier expansion and the geometry of the system, they can be expressed in terms of the structure factor for the PWE (EPWE) as well as for the PWE (EPWE) with supercell approximation. The index $i = (h, c)$ represents the host medium and the scatter respectively. The filling fraction of a cylinder in a supercell is $f = \pi r^2/A$, where A is the area occupied by the supercell. If we consider that β_i represents the values (ρ_i^{-1}, B_i^{-1}) , and that the supercell has N_c cylinders organized in an array of size $n_1 a \times n_2 a$ then

$$\beta(\vec{G}) = \begin{cases} \beta_c N_c f + \beta_h (1 - N_c f) & \text{if } \vec{G} = \vec{0} \\ (\beta_c - \beta_h) F(\vec{G}) & \text{if } \vec{G} \neq \vec{0} \end{cases} \quad (13)$$

where $F(\vec{G})$ is the structure factor of the supercell.

In this approximation the structure factor of the supercell has to be computed taking into account the size of the supercell. If we consider a 2D SC with cylindrical scatterers with radius r and size of the supercell $n_1 a \times n_2 a$, the structure factor of the supercell is expressed by

$$F(\vec{G}) = \sum_{i=-(n_1-1)/2}^{(n_1-1)/2} \sum_{j=-(n_2-1)/2}^{(n_2-1)/2} e^{i(a|\vec{G}_1| + ja|\vec{G}_2|)} P(\vec{G}) \quad (14)$$

where

$$P(\vec{G}) = \frac{2f}{Gr} J_1(G). \quad (15)$$

where a is the lattice constant inside the supercell and $G = |\vec{G}|$.

Previous equations show the expressions for the approximation of complete supercell. If the supercell presents N_p point defects at the sites labelled by (l_s, m_s) in the periodic system, with $s = 1, \dots, N_p$, then the Fourier coefficients of the expansions of the physical parameters involved in the problem follow the next equation

$$\beta(\vec{G}) = \begin{cases} \beta_c (N_c - N_p) f + \beta_h (1 - (N_c - N_p) f) & \text{if } \vec{G} = \vec{0} \\ (\beta_c - \beta_h) F(\vec{G}) & \text{if } \vec{G} \neq \vec{0} \end{cases} \quad (16)$$

The structure factor of such a supercell with N_p point defects is

$$F(\vec{G}) = \left(\sum_{i=-(n_1-1)/2}^{(n_1-1)/2} \sum_{j=-(n_2-1)/2}^{(n_2-1)/2} e^{i(a|\vec{G}_1| + ja|\vec{G}_2|)} - \sum_{s=1}^{N_p} e^{i(l_s a|\vec{G}_1| + m_s a|\vec{G}_2|)} \right) P(\vec{G})$$

The interaction of the defect points in the supercell approximation must be as low as possible between the neighboring supercells in order to decrease the overlap between defects, thus the size of the supercell should be big enough to place the point defects separated in consecutive supercells.

Introducing the previous expressions in the matrices of both the PWE (2) or the EPWE (11) we can calculate the real and complex band structures. In the present paper we analyze the case of a double-point defect in a square array at sites $(1, 0)$ and $(-1, 0)$

in a supercell of $11a \times 11a$. In this situation the distance between defects is equal to $2a$, and between two double-point defects in different supercells is equal to $20a$.

3. EPWE Results: Localized modes

Since Sigalas et al. [9] studied the defect mode produced by a point defect in periodic structures, several kinds of defects have been analyzed in the last years, showing in all cases the localization of sound for frequencies inside the BG [15, 27, 28]. Experimental and numerical analysis of the localization in a point defect considered as a cavity inside the SC have been reported recently by Wu et al. [29, 30] and by Zhao et al. [17, 31] showing the dependence of the localization on the size of the crystal and on the filling fraction (the bigger the size and the filling fraction the bigger the localization in the cavity). Moreover, when we consider two point defects, coupling between localized modes in each defect-point is possible [32, 33]. An accurate interferometric set up has been used by Russell et al. [33] for observing the coupled states in a double-point defect, noting the evidences for odd and even symmetry trapped states in new class of ultra-efficient photosonic devices in which both sound and light are controlled with great precision and their interactions enhanced. For the case of double-point defect, the bigger the distance between cavities the lower coupling between defect points.

In this section we show novel results about the imaginary part of the Bloch vector for the localized modes inside the SC with multi-point defects. The localization of waves inside these defects is mainly characterized by three properties. First, the modes are separated in the frequency domain, i.e., there is a splitting of the localization frequency if the point defects are close enough. Second, the modes present symmetries in the vibrational pattern depending on the number of vacancies in the crystal. Third, the localized modes are evanescent and they decays outside the defect but inside the SC. Without loss of generality we show results of a double point defect in very good agreement with the experimental data, showing the symmetric and antisymmetric vibrational pattern of the localized modes. Evidently, the oscillation modes of N -point defects with $N > 2$ will present more complicated vibrational patterns than the ones appearing in the double-point defect, then they cannot be classified into such simple modes as symmetric and antisymmetric ones.

The Complex and Real band structures reveal that the values of k for the localized modes are characterized by a real value of k and it is related with the localization frequency. However, this localized mode presents evanescent behaviour out of the defect because it is surrounded by a perfect periodicity, thus the excited mode in the surrounding crystal by the localized mode presents an imaginary k which is related with the evanescent behaviour of the mode outside the point defects [19]. The rest of modes inside the BG only present imaginary part, then they are killed inside the crystal because of their evanescent behaviour.

3.1. Splitting of localized modes

In order to analyze the splitting of the localized modes we have calculated the Real and the Complex Band Structures of a SC with a double point defect with the EPWE with the supercell approximation using a supercell of size $11a \times 11a$. We consider a 2D SC consisting of PVC cylinders of radius r in air background arranged in square lattice with lattice constant a . The material parameters employed in the calculations are $\rho_{air} = 1.23\text{kg}/\text{m}^3$, $\rho_{PVC} = 1400\text{kg}/\text{m}^3$, $c_{air} = 340\text{m/s}$ and $c_{PVC} = 2380\text{m/s}$. We consider a filling fraction $f = \pi r^2/a^2 \simeq 0.65$. For the calculations we have used $N = (2 \cdot 15 + 1)^2 = 961$ plane waves. Several calculations have been carried out in order to obtain a good convergence of the solution. This number of plane waves is bigger than the used in previous works [21] and it provides a good convergence of the solution of the eigenvalue problem.

A mode within the BG in an infinite SC without defects is characterized by a pure imaginary value of $k = \imath k_{im}$ (where $k_{im} = \text{Im}(k)$) [21, 19, 23]. In Figure 1a (left panel) we can observe the dependence of the $\text{Im}(k)$ on k for a complete SC within the BG for the ΓX direction. We can observe a maximum value of $\text{Im}(k)$ for the frequency in the midgap (926 Hz), that means the imaginary part of the wave number for frequencies inside the BG grows with values of frequency closer to the center of the BG and disappears at the edges of the BG, i. e., the rate of decay is bigger for frequencies closer to the center of the BG [7, 23, 19]. Modes within the BG decay inside the SC because of their evanescent behaviour [19].

In contrast to the modes in BG, localized modes can travel up to the point defect where the wave is localized. Figure 1a (central and right panels) represents the real band structures calculated by PWE with supercell approximation for both a SC with a point defect (central) and a SC with a double-point defect (right). We can observe the localized mode generated by a point defect in a SC at the frequency $\nu_0 = 932$ Hz whereas the frequencies of the localized modes of a double point defect have been split (right panel of the Figure 1a). The frequencies of the two localized modes due to the double-point defect split around the localized mode of a single defect: One with lower frequency, $\nu_1 = 910$ Hz, than the corresponding frequency of the localized mode in a single defect, and another one, $\nu_2 = 958$ Hz, with higher frequency than the single defect. This phenomenon is analogous to the splitting of the degenerate atomic levels in diatomic molecules.

The splitting in two peaks may be understood qualitatively by considering that the double cavity in the double-point defect are coupled forming a large cavity with two resonant frequencies. When a wave with one of these frequencies impinges on the crystal from outside, the double point defect is seen and the wave penetrates into the cavity. Then, the borders of the cavity act as a perfect mirrors producing the localization of the wave inside the cavity. This results in a coupling inside the double-point defect producing two localized modes depending on the distance between the point defects [15, 32, 17].

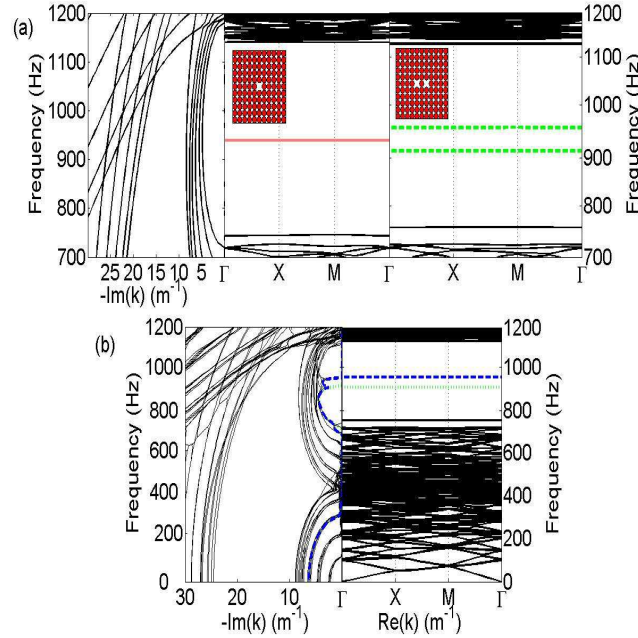


Figure 1. (Color Online) Real and Complex band structures for a SC with point defects. (a): Complex band structure of a complete SC calculated by EPWE with supercell approximation (left). Band structures calculated by PWE with supercell approximation of a SC with a point defect, the continuous red line represents the defect mode (center). Band Structures for a SC with a double-point defect, dashed green line represents the defect modes of a double point defect (right). Insets show the supercell used in the calculations. (b): Complex and real band structure of a double point-defect.

Because the splitting depends on the distance and on the shape of the multi-point defect, one can study the vibrational patterns that appear inside the multi-point defect, analyzing the differences in frequency of the localized modes. The factor $(\nu_1 - \nu_2)/\nu_0$ indicates how the splitting will be produced. For big values of this factor, one can expect modes separated in frequencies (as many as single-point defect constituting the multi-point defect), whereas a small factor represents a weak overlap between the point defects in the multi-point defect, which produces narrow splitting.

The complex band structures give us additional information about the properties of the localized modes. Figure 1b represents the complex (left panel) and the real (right panel) band structures for a SC with a double-point defect. For each localized mode a determined imaginary k becomes in a pure real value, in good agreement with the results of the PWE with supercell approximation. This real part is related with the wave vector for the localization frequency whereas the imaginary part of the localized mode is related with the rate of decay outside the defect but inside the SC. As we have seen, the localized modes in the double point defect are distributed around the localized mode of a single point defect. However, the localized mode of the single defect point appears a little above the midgap frequency (926 Hz). Thus it is expected that the imaginary part

of the localized modes of double-point defects present different values for each mode and, as a consequence, each mode presents different evanescent behaviour outside the defect (see Figure 1b). This prediction of the EPWE will be used for distinguishing experimentally the symmetric respect to the antisymmetric modes.

3.2. Symmetric and antisymmetric modes

The previous discussion about the splitting of the modes in multi-point defects does not provide information about how the modes are localized or what is the distributed field inside the double cavity. This will be discussed now.

The results obtained by the PWE or EPWE for the localized modes could be used to plot the modal shapes for the defect modes using the eigenvectors. However, these modal shapes do not take into account the effect of the finite size of the crystal. Thus, for comparing with experimental data corresponding to a SC of finite size, in this Section, we have calculated the modal shapes inside the double defect using Multiple Scattering Theory (MST). MST provides complementary information respect to the one provided by EPWE in the case of the infinite structures.

MST [34, 35] has been used to analyze the pressure field inside a SC with point defects. A SC of $7a \times 5a$ size with $a = 0.22\text{m}$ of rigid cylinders with radius $r = 0.1\text{m}$ is considered in this Section. We have generated a double-point defect with individual defect points separated a distance $d = 2a$. We have considered this size because of the experimental restrictions, and to be able to compare both theoretical and experimental data.

For the crystal considered in this Section the frequencies of the localization modes differs a bit respect to the calculated by PWE and EPWE with supercell approximation. We have to take into account that in this case we consider a finite crystal, and as it has been shown in the literature, the localization frequencies depend on the size of the crystal as well as the filling fraction, and the amount of rows around the defect. In this case, the localization frequency for the antisymmetric mode is $\nu_1 = 940\text{ Hz}$, and for the symmetric mode is $\nu_2 = 895\text{ Hz}$. These frequencies represent the maxima values of the acoustic spectra inside the point defects. Note the small difference respect to the obtained by PWE and EPWE.

The pressure fields calculated by MST inside the SC with a double-point defects for the localization frequencies are shown in the Figure 2. We can observe that the pressure field for the mode with high frequency has an antisymmetric pattern Figure 2a, whereas the pressure field for the mode with low frequency has a symmetric pattern Figure 2b.

In Figure 2 one can also observe the values of $|p|$ for the space between two rows of the SC containing the double-point defect. The vibrational patterns of the defect modes in double-point defect are characterized respect to a symmetry plane (see dashed line in Figure 2) situated just in the midpoint between the two defects in the double-point cavity. There is a symmetric mode and an antisymmetric mode respect this plane. The symmetric vibrational mode is characterized by a vibration in phase of the pressure field

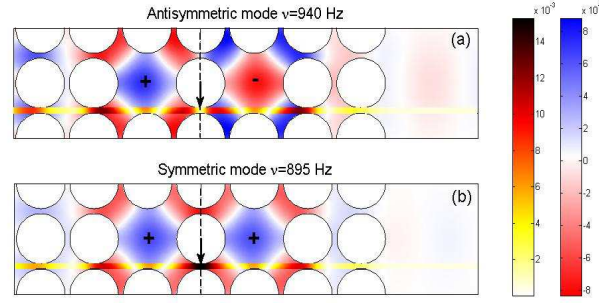


Figure 2. (Color Online) Pressure maps of a double-point defect separated a distance $d = 2a$. The value $|p|$ between two rows of the SC containing the point defects is also plotted. Pressure map of the antisymmetric (a) and symmetric (b) coupling of the localized modes inside the double-point defect. Arrow represents the values of $|p|$ in the midpoint (dashed line) between two rows of cylinders containing the double point defect.

in each point defect, whereas the antisymmetric mode is characterized by a vibration of the pressure field with opposition of phase. Because of these properties the point just in the symmetry plane presents different values of $|p|$ for each localized mode (see arrows in Figure 2). For the antisymmetric mode (Figure 2a) one can observe a minimum value of $|p|$ at this point, whereas one can find a maximum value for the symmetric mode (Figure 2b).

Experimental results inside the SC have been performed in an echo-free chamber of dimensions $8 \times 6 \times 3\text{m}^3$. In order to obtain the experimental dependence of the pressure all along the SC, we have measured the pressure field in several points between two rows of the SC containing the double-point defect. The experimental SC has been made of 1m long cylinders of PVC. The size of the SC considered in this work has the adequate dimensions to be capable to introduce the microphone between rows. The microphone used is a prepolarized free-field 1/2" Type 4189 B&K. The diameter of the microphone is 1.32cm, which is approximately $0.06a$, so the influence over the pressure field measured is negligible.

With our system 3DReAMS (3D Robotized e-Acoustic Measurement System) it is possible to sweep a 3D grid of measuring points located at any trajectory inside the echo-free chamber. Motion of the robot is controlled by NI-PCI 7334 . We have analyzed the absolute value of the sound pressure between two rows of the SC moving the microphone in steps of 1cm.

Figure 3 shows the values of $|p|$ obtained by MST versus the measured experimentally. The experimental results are in very good agreement with the obtained with MST. Note the different values of $|p|$ in the midpoint. As MST predicts, a maximum is observed for the symmetric mode at $\nu = 895\text{Hz}$, Figure 3b and a minimum for the antisymmetric mode at $\nu = 940\text{Hz}$, Figure 3a. The good agreement between theoretical (MST) and experimental results is remarkable. These measurements constitute the first

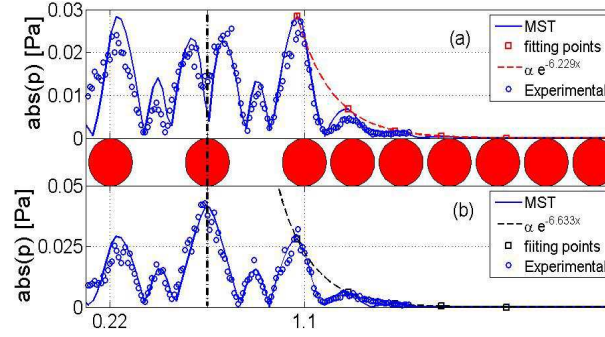


Figure 3. (Color Online) Numerical (continuous line) and experimental (open circles) profile of the $|p|$ between two rows containing the double-point defect (see Figure 2). (a) Antisymmetric mode ($\nu = 940\text{Hz}$) and (b) symmetric mode ($\nu = 895\text{Hz}$). Dashed line represents the exponential decay of the localized modes outside the double-point defect fitted from the maxima values of the analytical data represented with square open points. The border of the double-point defect is marked with a dotted line.

experimental evidence of the symmetric and antisymmetric vibrational modes inside the SC with a double point defect.

3.3. Decay of the localized modes

Due to the mode of a single point defect is a little above of the midgap, one can observe in Figure 1b that the localized modes in a double point defect present different imaginary part of k : The values of the imaginary part of k for the antisymmetric mode are lower than the corresponding for the symmetric mode, i.e., the rate of decay outside the cavity of the symmetric mode must be bigger than that of the antisymmetric case. In Figure 3 one can observe the decay of the localized modes outside the double-point cavity. The border of the double point defect are marked by dotted lines.

In order to analyze the decay of the modes outside the cavity, we have studied the behaviour of the maximum analytical values of $|p|$ outside the cavity (see open squares in Figure 3), calculated by MST in a SC of rigid cylinders with size $11a \times 5a$. Although the decay of the modes outside the cavity is multiexponential [18], we can fit this values to an exponential-like ae^{bx} for analyzing the differences in the rate of decay due to the differences in the imaginary part of the k for each localized modes.

Both fitted exponential decays are represented in the Figure 3 (dashed lines). The decay rate for the antisymmetric mode is $b = -6.229 \pm 0.237 \text{ m}^{-1}$, while the decay rate for the symmetric mode is $b = -6.633 \pm 0.178 \text{ m}^{-1}$. Thus, as it was discussed in the results obtained in previous section by EPEWE with supercell approximation, because of the symmetric distribution of the frequencies of the localized modes in double point defect respect to the localized mode in a single cavity, the decay rate of the antisymmetric mode in a double-point defect must be lower than that of the symmetric mode. On the other hand, we can observe that the values of the decay rate of the symmetric and of the antisymmetric modes are similar and the difference between them is small. The

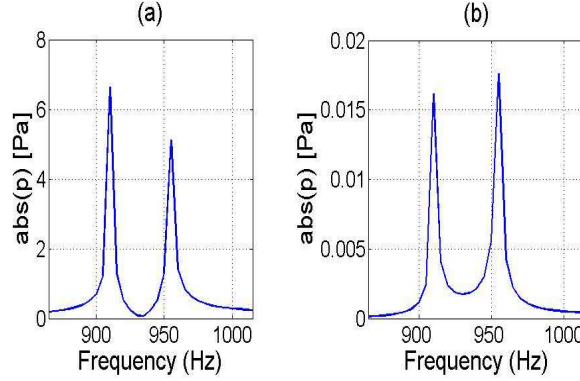


Figure 4. (Color Online) Spectra for a SC made of PVC $9a \times 5a$ cylinders with a lattice constant $a = 0.22\text{m}$ in square array with a double-point defect. (a) Spectrum measured inside one of the point-defect in the double point defect. (b) Spectrum measured outside the crystal at a distance $10a$ from the start of the SC.

splitting of the frequencies of the localized modes in a double point defect around the frequency of the single cavity, implies that the rate of decays in double point defect have to be different, but also one of them should be smaller than the other because its distance to the center of the gap is bigger.

In finite crystals, where the localized modes can travel outside the periodic structure because of their evanescent behaviour, the previous results indicate that the symmetric mode will be killed more easily than the antisymmetric mode. Thus, the design of filters based on SC with point defect should take into account this kind of results. In Figure 4a we represent the spectrum inside a point defect in a SC with a double-point defect. In this case, we can observe that the value of pressure of the peak of the symmetric mode (lower frequency) is higher than the peak of the antisymmetric mode. In Figure 4b we represent the spectra for the same SC with a double-point defect but measured outside the SC at a distance $10a$ from the beginning of the SC. We can observe that the values of pressure for the symmetric mode are lower than the values of the antisymmetric mode, thus the symmetric mode has been more damped by the crystal out of the double-point defect than the antisymmetric mode. Similar results can be observed in Figure 2, where the acoustic field behind the crystal for the antisymmetric mode is a bit bigger than the corresponding for the symmetric mode. These results are in complete agreement with the differences in the imaginary part of k . Moreover, the difference in the value of imaginary of complex wave vector is a direct evidence of the existence of different vibrational modes in multi-point defects and reveals the existence of a coupling between them.

4. Conclusions

Usual calculations with Plane Wave Expansion, $\omega(k)$ methods, do not provide any information about the evanescent behaviour of the localized modes in point defects

inside periodic structures. In this work we present the explicit matrix formulation of the Extended Plane Wave Expansion (EPWE) with the supercell approximation for a supercell with N_p point defects for SC. This technique allows us to study the evanescent behaviour of the modes inside SC with multipoint defects. Localized modes in SC are mainly characterized by three properties: splitting of frequencies, the symmetry of the vibrational patterns and evanescent behaviour inside the crystal. EPWE in addition to PWE both with supercell approximation have been used to analyze the whole properties of the localized modes in a SC with a double point defect. First we analyze the splitting produced by the generation of a double-point defect, showing the effects in both the real and imaginary band structures. From the imaginary complex band structure we obtain that the localized modes present different values for the imaginary part of k , that means each mode has a different decay rate inside the crystal. This property has been observed experimentally by fitting the exponential decay for each localized mode inside the crystal. The symmetry of the vibrational patterns in double-point defect have also been analyzed in the paper by means of MST calculation and experimental data. Novel experimental evidences show the symmetric and antisymmetric vibrational patterns in SC with double-point defects. These data are in very good agreement with analytical data. Finally, using the different decay rate of both vibrational modes, we confirm our conclusions giving a new methodology to determine different vibrational modes in periodic media. This work shows the basis for the correct understanding of the design of narrow filters and wave guides based on periodic structures with multi-point defects.

Acknowledgments

This work was supported by MEC (Spanish Government) and FEDER funds, under grants MAT2009-09438 and MTM2009-14483-C02-02.

References

- [1] Sigalas M and Economou E 1993 *Solid State Commun.* **86** 141
- [2] Kushwaha M, Halevi P, Dobrzynski L and Djafari-Rouhani B 1993 *Phys. Rev. Lett.* **71** 2022–2025
- [3] Yablonovitch E 1987 *Phys. Rev. Lett.* **58** 2059
- [4] John S 1987 *Phys. Rev. Lett.* **58** 2486
- [5] Martínez-Sala R, Sancho J, Sánchez-Pérez J V, Gómez V, Llinares J and Meseguer F 1995 *nature* **378** 241
- [6] Khelif A, Wilm M, Laude V, Ballandras S and Djafari-Rouhani B 2004 *Phys. Rev. E* **69** 067601
- [7] Joannopoulos J D, Johnson S G, Winn J N and Meade R D 2008 *Photonic Crystals. Molding the Flow of Light* (Princeton University press)
- [8] Sigalas M, Kushwaha M S, Economou E N, Kafesaki M, Psarobas I E and Steurer W 2005 *Z. Kristallogr.* **220** 765–809
- [9] Sigalas M 1997 *J. Acoust. Soc. Am.* **101** 1256
- [10] Sigalas M 1998 *J. Appl. Phys.* **84** 3026
- [11] Sánchez-Pérez J V, Rubio C, Martínez-Sala R, Sánchez-Grandia R and Gómez V 2002 *Appl. Phys. Lett.* **81** 5240

- [12] Vasseur J O, Deymier P A, Djafari-Rouhani B, Pennec Y and Hladky-Hennion A C 2008 *Phys. Rev. B* **77** 085415
- [13] Kushwaha M, Halevi P, Martinez G, Dobrzynski L and Djafari-Rouhani B 1994 *Phys. Rev. B* **49** 2313–2322
- [14] HHernández-Cocoletzi, AKrokhin and PHalevi 1995 *Phys. Rev B* **51** 17181–17183
- [15] Li X and Liu Z 2005 *Solid State Communications* **133** 397402
- [16] Wu F, Hou Z, Liu Z and Liu Y 2001 *Phys. Lett. A* **292** 198
- [17] Zhao Y and LBYuan 2009 *J. Phys. D: Appl. Phys.* **42** 015403
- [18] Engelen R, Mori D, Baba T and Kuipers L 2009 *Phys. Rev. Lett.* **102** 023902
- [19] Romero-García V, Sánchez-Pérez J V, Castiñeira Ibáñez S and Garcia-Raffi L M 2010 *Appl. Phys. Lett.* **96** 124102
- [20] Hsue Y, Freeman A and Gu B 2005 *Phys. Rev B* **72** 195118
- [21] Laude V, Achaoui Y, Benchabane S and Khelif A 2009 *Phys. Rev. B* **80** 092301
- [22] Romero-García V, Sánchez-Pérez J V and Garcia-Raffi L M 2010 *arXiv:1001.3758*
- [23] Wang Y, Li F, Kishimoto K, Wang Y and Huang W 2009 *Eur. Phys. J. B.* **67** 501–505
- [24] Sainidou R, Stefanou N, Psarobas I and Modinos A 2005 *Computer Physics Communications* **166** 197–240
- [25] Psarobas I E, Stefanou N and Modinos A 2000 *Phys. Rev. B* **62** 278
- [26] Sainidou R and Stefanou N 2006 *Phys. Rev. B* **73** 184301
- [27] Wu F, Zhong H, Zhong S, Liu Z and Liu Y 2003 *Eur. Phys. J. B* **34** 265–268
- [28] Zhong H, Wu F, Zhang X and Liu Y 2005 *Physics Letters A* **339** 478–487
- [29] Wu L, Chen L and Liu C 2009 *Physica B* **404** 1766
- [30] Wu L Y, Chen L W and Liu C M 2009 *Phys. Lett. A* **373** 1189–1195
- [31] Zhao Y C, Wu Y B and Yuan L B 2009 *Phys. Scr.* **80** 065401
- [32] Khelif A, Choujaa A, Djafari-Rouhani B, Wilm M, Ballandras S and Laude V 2003 *Phys. Rev. B* **68** 214301
- [33] Russell P S J, Marin E, Dez A, Guenneau S and Movchan A B 2003 *Opt. Expr.* **11** 2555
- [34] Linton C and McIver P 2001 *Handbook of Mathematical Techniques for Wave/Structure Interactions* (Chapman and Hall/CRC (Florida))
- [35] Chen Y Y and Ye Z 2001 *Phys. Rev. E* **64** 036616